The Full-Size Source and Injector Prototypes for ITER Neutral Beams*)

Gianluigi SERIANNI, Piero AGOSTINETTI, Vanni ANTONI, Daniele APRILE, Carlo BALTADOR, Marco CAVENAGO[1)], Giuseppe CHITARIN, Nicolo' MARCONATO, Diego MARCUZZI, Emanuele SARTORI, Piergiorgio SONATO, Vanni TOIGO, Pierluigi VELTRI and Pierluigi ZACCARIA

Consorzio RFX (CNR, ENEA, INFN, UNIPD, Acciaierie Venete SpA), Corso Stati Uniti 4-35127 Padova, Italy
[1)]*INFN-LNL, viale dell'Università n. 2, 35020 Legnaro, Italy*

(Received 1 December 2015 / Accepted 5 April 2016)

The development of the NBI systems for ITER requires unprecedented parameters (40 A of negative ion current accelerated up to 1 MV for one hour) so that a test facility is in the final phase of construction at Consorzio RFX (Padova, Italy), housing two experiments. A full-size negative ion source, SPIDER, aims at demonstrating the creation and extraction of a D-/H- current up to 50/60 A on a wide surface (more than 1 m^2) with uniformity within 10 %. The second experimental device is the prototype of the whole ITER injector, MITICA, aiming to develop the knowledge and the technologies to guarantee the successful operation of the two injectors to be installed in ITER, including the capability of 1 MV voltage holding at low pressure. The key component of the system is the beam source, whose design results from a trade-off between requirements of the optics and real grids with finite thickness and thermo-mechanical constraints due to the cooling needs and the presence of permanent magnets. Numerical simulations are a necessary supplement to the experimental effort to optimise the accelerator optics and to estimate heat loads and currents on the various surfaces.

In this paper the main requirements for ITER NBI will be discussed. The design and the status of the main components and systems will be described. Particularly a review of the accelerator physics and a comparison between the designs of the SPIDER and MITICA accelerators are presented. Complex network theory will be applied to the NBI system in order to identify the hidden functional relationships and the most important parameters for the operation.

Keywords: neutral beam injector, plasma heating, systems theory

DOI: 10.1585/pfr.11.2402119

1. Introduction

Two Neutral Beam Injectors (NBI) will provide a substantial fraction of the heating power necessary to ignite thermonuclear fusion reactions in ITER. The development of the NBI systems at unprecedented parameters (40 A of negative ion current accelerated up to 1 MV continuously operating for one hour) requires a strong demonstration activity, which was endorsed by ITER to optimise the crucial components and systems. A test facility, PRIMA (Padova Research on ITER Megavolt Accelerator), is presently in the final phase of construction at Consorzio RFX (Padova, Italy) in the CNR research area and will house two experiments, named SPIDER and MITICA. SPIDER (Source for the Production of Ions of Deuterium Extracted from Rf plasma), the full-size negative ion source, will demonstrate the creation and extraction of a D^-/H^- current up to 50/60 A on a wide surface (more than 1 m^2) with uniformity within 10 %. The second experimental device is the prototype of the whole ITER injector, MITICA (Megavolt ITer Injector and Concept Advancement), aiming to develop the knowledge and the technologies to guarantee the successful operation of the two injectors to be installed in ITER, including the capability of 1 MV voltage holding at low pressure, and steady state operation up to one hour. The beam source is the key component of the system, whose design results from a trade-off between requirements of the optics and real grids with finite thickness and thermo-mechanical constraints due to the cooling needs and the presence of permanent magnets. The experimental effort is supplemented by numerical simulations devoted to the optimisation of the accelerator optics and to the estimation of heat loads and currents on the various surfaces.

The design of SPIDER and MITICA constitutes a challenge from the physical and the technological point of view; in the first part of this paper, the main components will be described, by breaking the system up into

author's e-mail: gianluigi.serianni@igi.cnr.it

*) This article is based on the invited presentation at the 25th International Toki Conference (ITC25).

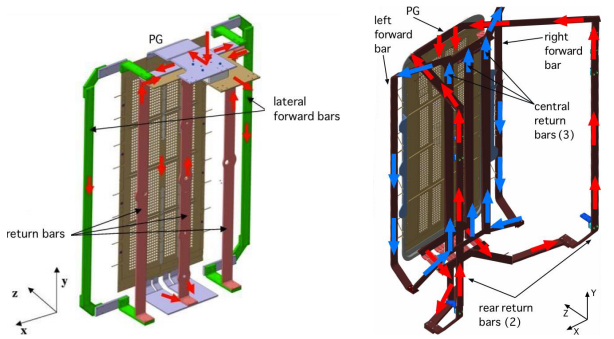

(a) SPIDER (b) MITICA

Fig. 1 Final PG busbar design for SPIDER (a), and MITICA (b).

its main elements and by grouping them by functionality, while proposing some examples of adopted solutions. The very operation of such prototypes is challenging, for the complex cause-effect relations among all aspects; in the second part of the paper, an opposite point of view is offered, by giving a unitary view of the subsystems, based on a network of functional relationships. In view of the start of the experimental operations, such a network can become a powerful tool supporting the experimentalists. It can also orient the choices related to diagnostics and measurements, steering the experimental effort towards more promising paths.

2. SPIDER and MITICA: Physical Issues and Design Description

Even though particle beams have been used in fusion applications since 1973 [1], the detail design for the ITER neutral beam has been challenging. While in no way pretending to be exhaustive, in the following key aspects of the design are summarised.

The final design of the ITER NBI, a result of about four years of continuous development involving a team of engineers and physicists belonging to Consorzio RFX and other research institutes, permits to satisfy all the performance requirements together with the voltage holding and mechanical verifications [2]. The final design of the accelerator can be considered versatile because the performance in terms of beam optics is acceptable also when the current extracted from the RF ion source or the heat loads on the grids are different, but within a reasonable range, from the target parameters [3, 4]. The adoption of optimized shapes of the grid supporting frames and filleted edges of the grid apertures have permitted to improve the voltage holding capability, while the adoption of kerbs and a careful grid shaping have permitted to focus the beam as required in ITER. A combination of long-range (produced by currents – Fig. 1 and Fig. 2) and short-range magnetic fields (due to permanent magnets – Fig. 3 - Fig. 5) has permitted to effectively dump the stripped electrons on the acceleration grids reducing the heat load concentration and helping to fairly

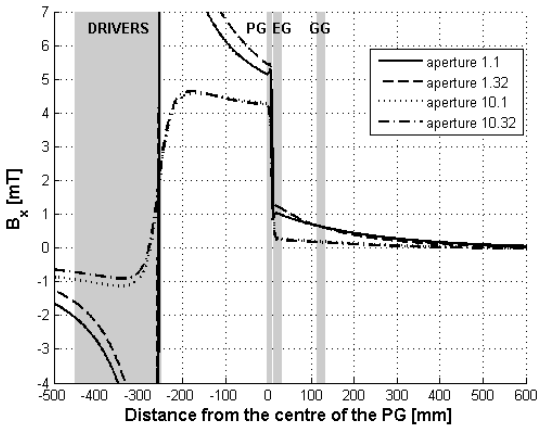

(a) SPIDER

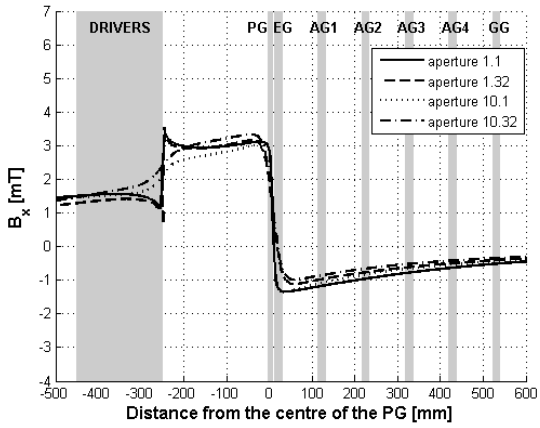

(b) MITICA

Fig. 2 Profiles of transverse horizontal field B_x generated by current flowing in Plasma Grid and related busbar system. Paths are numbered so that: (1,1) is the top left of the grid; (1,32) top centre; (10,1) middle left; (10,32) middle centre.

share the heating power among the grids.

Finally, three completely new solutions have been introduced, the Asymmetric Deflection Compensation Magnets (ADCM), providing a suitable compensation of the Criss-Cross Deflection Effect in all operating scenarios, the Nozzle Island Cooling Enhancement (NICE) for the grids, providing a high performance cooling without exceeding the limits on the pressure drop through the grids, and the Stress Relieving Slits (SRS), reducing the stress due to thermal gradients through the grids. The combination of NICE and SRS have permitted to increase the fatigue life of the grids from less than 3000 to more than 100000 beam on-off cycles, satisfying the ITER requirements with a large margin.

2.1 Background gas density

One prerequisite for beam simulation is the knowledge of the background gas pressure distribution: it is at the origin of beam losses via stripping and stray particle creation in the accelerator, and causes further beam losses

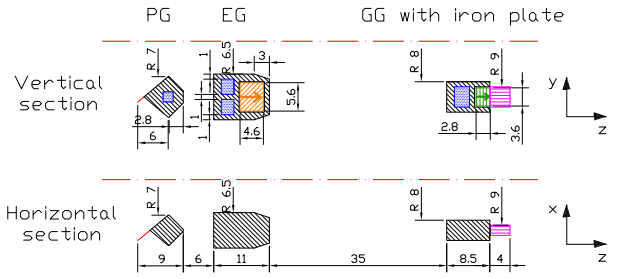

Fig. 3 Vertical cross section of the SPIDER accelerator grids, showing the Co-extracted Electrons Suppression Magnets (CESM) permanent magnets (orange and green), the water cooling channels (blue) and the ferromagnetic layer (magenta).

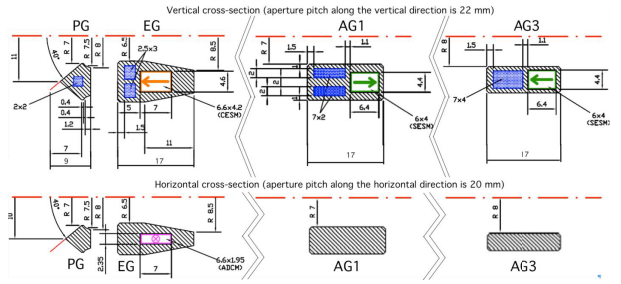

Fig. 4 Cross section of the acceleration grids of MITICA: PG, EG, AG1 and AG3. The AG2 is identical to AG1 and AG4 is identical to AG3. The GG is also identical to AG3, but has no magnets.

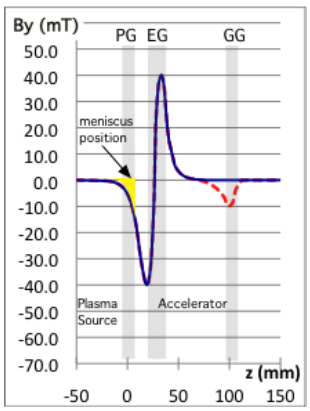

(a) SPIDER

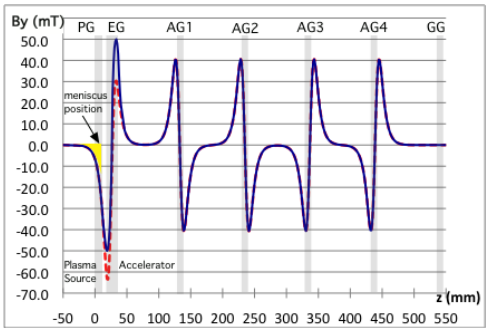

(b) MITICA

Fig. 5 Profile of the transverse vertical field B_y produced by electron suppression magnets embedded in the accelerator grids of SPIDER and MITICA (solid blue line). The dashed red lines indicate the adjustments for compensating the magnetic deflection caused by the meniscus position.

by reionisation at the downstream of the neutraliser. Furthermore, in the case of MITICA the beam source and beam line are an integrated system from the vacuum point of view: the conditions in the accelerator affect the beam line and vice-versa. For what concerns the beam source, the hydrogen isotope in the ion source is provided at a fixed gas flow, such that in the absence of plasma the filling pressure is as high as 0.3 Pa in the case of deuterium and 0.45 Pa in the case of hydrogen. The geometry of the extractor and accelerator, including the support frames, has been characterised, by the angular coefficient approach, with the Avocado code [5] for both the case of SPIDER [6] and MITICA [7]. For the latter case, numerical modelling helped in optimizing the frame geometry to maximize the pumping speed in between the grids [8], and was constantly used to support the design by evaluating the impact of geometrical changes on the gas density; specific problems were addressed, such as the transversal gas density non-homogeneity that can impact on beamlet currents and perveance [9]. The case of the gas flow out of the ion source is highly influenced by the temperature variation, from around 1150 K down to the electrode temperature. Numerical models of low-pressure gas flows in non-isothermal regime require the knowledge of the accommodation coefficient to describe these phenomena; for the specific problem of SPIDER and MITICA, a molecular dynamics model was developed to characterize the H_2/D_2 particle impact on a copper surface [10]. An example of design solution that can affect the gas flow in the beamline is the use of an electron dump made of extensive copper panels, installed to protect the cryopump [11]. Its influence in the pumping speed at the beam source was studied and minimized, causing only a minimal pressure increase (below 20 %) in the drift region between the beam source and the neutralizer.

2.2 Magnetic fields

A transverse magnetic field in the ion source and accelerator [12] is necessary both in SPIDER and in MITICA for the following reasons :

- in the Ion Source: a “Filter Field” on the upstream side of the Plasma Grid (PG) is required for reducing the average energy of electrons approaching the grid and for optimizing the extraction of the negative ions [13]. According to the recent ELISE results, the optimal “Filter Field” for ion extraction varies between 2 mT and 4 mT, depending on the ion species (H^- or D^-). The start-up and sustainment of the plasma in the RF drivers can be hampered if the “Filter Field” penetrates inside the driver

antennas [14].

- in the Accelerator: a local "Suppression Field" on the downstream side of the PG is necessary for eliminating the co-extracted electrons. As in most of the existing experiments, the Suppression Field is generated by arrays of permanent magnets embedded in the Extraction Grid (EG) and has two opposite peaks of about 50 - 60 mT along each beamlet, in order to reduce the resulting deflection of the ions [15]. However, this field can degrade the final beam optics by introducing a zig-zag deflection of some mrad on the ion beamlets. This deflection has to be compensated for [16].

In the case of the multi-stage MITICA accelerator some additional issues exist:

- a long-range "Suppression Field" of about 1.5 mT on the downstream side of the PG and in the whole accelerator is necessary for an immediate deflection of the electrons generated by stripping reactions of negative ions with background gas, before they are accelerated to higher energy. This field reduces the number of electrons and the associated loads on the beam line components at the accelerator exit (neutralizer, residual ion dump, cryopumps). However, the long-range Suppression Field can also concentrate the electron heat load on small portions of the intermediate grids AG1-AG4 and therefore increase the associated thermo-mechanical stress [17, 18].
- a local "Suppression Field" produced by permanent magnets embedded inside the acceleration grids AG1-AG4 is required in combination with the above mentioned long-range field, for an efficient disposal of the power carried by the electrons generated by stripping reactions. The layout and strength of the AG1–AG4 magnets is the result of many optimization cycles aimed at driving the electrons to impinge as close as possible to the cooling channels on the grids [19].
- the MITICA injector design is based on the PG current as the only source for the production of both the "Filter Field" in the ion source and the long-range "Suppression Field" in the accelerator. The ratio between the strength of these fields is fixed by the geometry of the PG busbars so as to match both the "optimal" magnetic field value in the Accelerator (~1.5 mT, based on extensive numerical simulations made by RFX and CEA) and in the Plasma Source (~4 mT, based on the available results obtained at IPP [13, 14]).

Both numerical simulations and experiments have shown that the Suppression Field produced by the magnets in the EG introduces a considerable deflection on the beamlets. As the direction of B_y is alternate row by row, a zig-zag deflection up to some mrad affects the accelerated ion beamlets [16], which can degrade the overall beam optics. To a first approximation, the ion deflection produced by the B_y suppression field depends on the integral $\int_{z_{start}}^{z_{exit}} B_y dz$ along the ion acceleration path. By modifying the B_y profile along the accelerator, the integral of B_y along the ion trajectory can be adjusted so that the final ion deflection is reduced or cancelled (the additional electrostatic-lens effect, which is not negligible when a beamlet is not coaxial with the grid apertures, must also be included in this calculation).

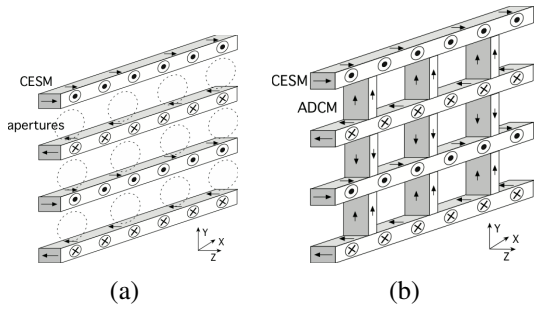

Fig. 6 (a) standard EG magnet layout in multi-aperture negative ion Accelerators (such as SPIDER); (b) MITICA EG magnet layout, including the Asymmetric Deflection Compensation Magnets (ADCM).

In SPIDER the B_y profile modification is attained by introducing an additional set of permanents magnets and a 4 mm thick ferromagnetic plate in the GG, as shown in Fig. 3. The magnets have a cross-section of 2.8×3.6 mm and are oriented as in the EG. Since the magnetic field lines on the downstream side are channelled through the ferromagnetic plate, the second peak of the magnetic field generated by the GG magnets is eliminated as shown in Fig. 5a (red dashed line), so as to produce the necessary asymmetry for the compensation of the ion deflection.

For MITICA, a new method to cancel the magnetic deflection has been conceived, which corrects the deflection as soon as it initiates (at the EG) and does not involve ferromagnetic materials. An additional set of small permanent magnets, arranged as shown in Fig. 6b, is embedded in the EG. These magnets, called Asymmetric Deflection Compensation Magnets (ADCM) "concentrate" the transverse vertical field B_y on the upstream side of the EG and therefore modify the B_y profile as shown in the red dashed line in Fig. 6b. The B_x component produced by the ADCM is several orders of magnitude smaller than B_y (less than 10 - 4 mT).

To summarise, the magnetic design of SPIDER and MITICA is based on the latest indications from the experimental devices at IPP and JAEA, as well as on the outcome of the numerical beam optics simulations. Moreover, the zig-zag magnetic deflection of the accelerated ions is intrinsically compensated for in a robust voltage-independent manner, and the leakage field in the RF drivers is within safe limits.

2.3 Particle trajectories and heat loads

The beam transport inside the accelerator is crucial in defining the divergence of the 1280 beamlets. A minimum divergence (<7 mrad) is necessary to guarantee the propagation of the beams along the 25 m long path from the

accelerator to the ITER plasma without any interception with the "walls". The divergence can be controlled by a careful shaping of the electrostatic lenses which are formed at each aperture of the grids, balancing the current density of the beamlet with the electrode profiles and the grid voltages. The modelling of these phenomena was carried out by means of beam trajectory codes, capable of solving the Poisson equation coupled with the motion equation in a self-consistent manner, with the adoption of an iterative approach.

The 2D axial symmetric code SLACCAD [20,21] was applied to design the electrode shape and gap length of both SPIDER and MITICA, using several combinations of extracted currents and electrode voltages. This code simulates a single beamlet only, with poor or no assumptions on the effect of large scale structures or surrounding beamlets. Therefore, in a second phase the 3D and multi-beamlet effects can be taken into account, by exploiting the results of the SLACCAD calculations. This reduces the number of parameters to be explored in the time consuming 3D analyses, allowing working directly with quasi-cylindrical beamlets. This set of 3D simulations was performed with the OPERA code [22], employed to follow the ion trajectories in the presence of the magnetic field, taking into account the effect of beamlet-beamlet interaction and the additional electrostatic push given by the shape of grid support structures. In the case of SPIDER, all beamlets are required to leave the accelerator following the same direction, i.e. perpendicular to the last accelerating electrode. Therefore the only effect that needs to be compensated for is the repulsion among beamlets. This is achieved by applying the displaced aperture technique [23] to the grounded grid apertures [24]. In the case of MITICA, on the other hand, the beamlets are required to leave the accelerator with specified aiming in the vertical and horizontal planes, in order to focus the beam at 25 m. To impress the required steering, electrodes are shaped as concave surfaces so as to deform the electric field consequently [25]. Additional field electrode plates (called kerbs) are also added for a more precise control of the beamlet trajectories. The fields calculated with these codes are then used to evaluate the interaction of the beam with the metallic electrodes, and with the background gas, both resulting in the production of secondary particles. For this task a Monte Carlo model was used [26] whose main outcome is the evaluation of the power loads on the different electrodes of the accelerator, which is necessary to dimension the cooling systems. Finally, the beam transport in the drift region after the accelerator was evaluated with Particle-In-Cell (PIC) codes to simulate the space charge compensation phenomena [27, 28] and with Monte Carlo beam trajectory codes for beam-gas and beam-surface interactions [29,30]. These codes have to be validated by comparison with experimental data, which can be accomplished using spatially refined measurements and dedicated simulations [31, 32].

2.4 Thermo-mechanical design and effect of heat loads

The themo-mechanical design of the ITER NBI must fulfil the following requirements:

- A peak temperature lower than a reference limit of 200°C [33];
- Stress distribution and fatigue life satisfying the criteria imposed by ITER SDC-IC (Structural Design Criteria for In-Vessel Components) criteria;
- Acceptable alignment among all the grids in a suitable range of operating scenarios.

To meet these requirements, the design of the grids has been studied by means of three-dimensional fully self-consistent fluid-thermal-structural models. Since the first simulations, it was clear that the most critical of these requirements was the one regarding fatigue life, while the other requirements were easily satisfied. In fact, the expected fatigue life was significantly lower than the required one owing to the high thermal stress caused by the huge heat loads deposited on the accelerator grids by the beam and the related particles generated by stripping and ionization reactions.

Two novel design improvements have been introduced to improve the thermo-structural behaviour of the grids: the Nozzle Island Cooling Enhancement (NICE), able to provide a high performance cooling without exceeding the limits on the pressure drop through the grids, and the Stress Relieving Slits (SRS), able to reduce the stress due to thermal gradients through the grids. Thanks to the NICE and SRS concepts, the ITER NBI now fully satisfies the requirements [2].

2.5 Grid system: focus on extractor and accelerator

The extraction and acceleration system for the MITICA beam source [34] is composed of seven grids: the Plasma Grid (PG), the Extraction Grid (EG), four acceleration grids (AG1-AG4) and the Grounded Grid (GG). The first two represent the extraction system, the following five the acceleration system. All the grids are approximately 1600 mm high and 800 mm wide (divided into four segments of about 400 mm × 800 mm for alignment and manufacturing reasons). Each grid features 1280 apertures (320 per segment), grouped in sixteen beamlet groups made of 16 × 5 apertures, where the ion beamlets are extracted from the ion source and accelerated up to 1 MeV, forming an ion beam of the required 40 A at the exit.

The Radio Frequency (RF) ion source is the component where the negative ions (H^- or D^-) are generated [35].

A voltage of about +9 kV is applied between the PG and the EG, so that, in the vicinity of the PG apertures, the electric field extracts the negative ions from the ion source toward the EG. The ions are then accelerated, in 5 stages, to full energy (1 MeV) by the effect of the AG1, AG2, AG3, AG4 and the GG, whose electric potentials are −800, −600, −400, −200 and 0 kV respectively.

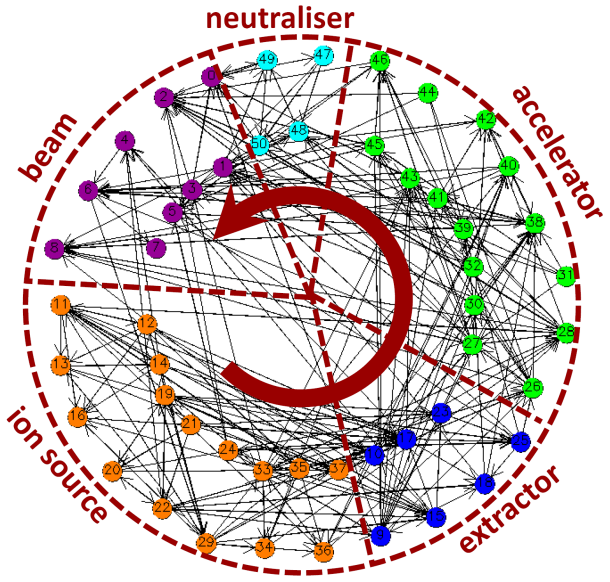

Fig. 7 Geography of the NBI directed graph. The arrows indicate the path of one hydrogen/deuterium atom from generation to full acceleration and neutralization.

The grids contain embedded permanent magnets and cooling channels. The former are used to deflect onto the grids the electrons that are accelerated together with the negative ions inside the accelerator, the latter to exhaust the heat loads on the grids that are caused by energetic particles inside the accelerator (electrons, negative ions, positive ions and neutrals that impinge on the grids).

The grid segments feature a rather complex design with very small cooling channels that run inside the grid and grooves for embedded magnets. Moreover, they are not flat but have machined areas around the groups of apertures so that the beam generated by each group is inclined horizontally towards the beamline axis.

3. Functional Analysis of NBIs

For an NBI to operate, negative ions shall be produced accelerated and neutralized, while maintaining a good beam optics and guaranteeing the survival of mechanical components. The detailed breakdown of this very clear and simple structure allows to enumerate all the functionalities required of each subsystem [36]. Most importantly it allows to identify cross-relations among all these, by constructing a graph. In the following, the functions of the main elements are described and the desired outputs in terms of beam properties; the items in the NBI functional graph are shown in Fig. 7; the definition of the nodes is found in Table 1.

Ion source (orange nodes):
–Generation of plasma
–Dissociation of hydrogen
–Acceleration of hydrogen atoms towards PG
–Caesiation of PG
–Generation of negative ions via caesiated PG

Extractor and Accelerator (blue and green nodes):
–Extraction of negative ions
–Dumping of co-extracted electrons
–Acceleration of beam
–Aiming and focussing beam

Neutralizer (light blue):
–Transport of beam (space charge compensation)
–Neutralisation of beam

Table 1 Definition of NBI graph nodes. Bold and underlined items are driver nodes (see text).

0	H0_flow_after_neutralizer
1	Divergence
2	Beam_aiming
3	Beam_particle_energy
4	j_e/j_H-
5	Beam_disuniformity
6	Temperature_of_mechanical_components
7	Fatigue_life
8	Accelerator_breakdown
9	I_H-_ext:_extracted_current
10	n_H/n_H2_dissociation_fraction_in_extraction_region
11	Source_Pressure
12	Gas_temperature_in_Driver
13	Electron_pdf_in_driver
14	Hot_Electron_temperature_in_extraction_region
15	Cold_Electron_temperature_in_extraction_region
16	Energy_of_H0_impinging_on_PG
17	n_H-_in_extraction_region
18	Meniscus_shape/Focal_length
19	Caesium_volume_density_during_pulse
20	Caesium_volume_density_off-pulse
21	Injected_Caesium_flux
22	Caesium_monolayer_number/Work_function
23	Caesium_layer_disuniformity
24	Plasma_drifts
25	Beam_disuniformity_at_meniscus
26	I_H-_EG
27	I_H-_acc
28	n_H2_accelerator
29	n_H2_source
30	EG_lens_(Focal_length)
31	AG_lenses_(Focal_length)
32	GG_lens_(Focal_length)
33	n_H2_PG-EG
34	T_H2_PG-EG
35	Gas_temperature_in_Expansion_region
36	n_H0_PG-EG
37	Caesium_in_PG-EG
38	Secondary_Electrons_emitted_at_surfaces
39	Beam_disuniformity_at_EG_exit
40	Secondary_Electrons_in_PG-EG
41	Secondary_Electrons_in_accelerator
42	Leaking_Secondary_Electrons
43	Back-Streaming_Positive_Ions
44	Deflection_of_H-_in_PG-EG
45	Deflection_of_H-_in_accelerator
46	Deflection_of_H-_after_GG
47	n_H2_neutralizer
48	Space_charge_compensation_after_GG
49	Geometrical Transmission of Beam through Neutralizer
50	n_H2_vessel

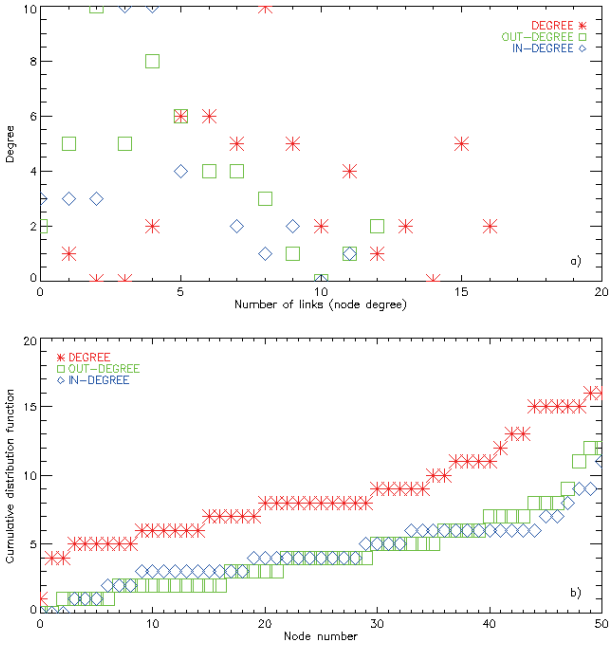

Fig. 8 Histogram of node degrees (a) and cumulative degree distribution (b).

–Dumping of residual ions
Beam parameters and NBI operation:
–neutral beam energy,
–current,
–divergence and aiming
–component temperature within design limits.

3.1 NBI graph statistics

The graph shown in Fig. 7 is a directed graph [37], having $m = 51$ nodes, with 407 weighed interconnections (edges) a_{ij}. The procedure to create the directed graph consists in identifying, for each node, which other nodes affect its behaviour (*causal* relations), attributing a coefficient c_{ij} according to the strength of this relationship, and use c_{ij} to populate a sparse $m \times m$ matrix; the edge weights a_{ij} are obtained by normalizing to one the summation by row, as $a_{ij} = c_{ij} / \sum j c_{ij}$. All weights range from 0.125 % to 55 %, but negligible weights ($a_{ij} < 3$ %) have been neglected in this study, leaving 222 edges. The distribution of the node degrees (number of edges connected to one node) for the NBI graph is shown in Fig. 8a: it ranges from 1 to 16. Compared to graph representing common systems, this network is strongly interconnected, displaying very few nodes with low degree and a high average node degree (4.35), meaning that on average each node is connected to 8.7 % of all nodes. The node relations are balanced in the sense that the cumulative distribution of out-degrees and in-degrees (Fig. 8b) are balanced, being also in the same range (respectively 0 - 12, and 0 - 11).

A standard operation on graphs is clustering. Clusters correspond to nodes functionally linked, and can highlight notable phenomenology. A preliminary example of clustering analysis based on Markov search [38], which finds a community of nodes tightly connected among themselves, is shown in Fig. 9, computed by Gephi [39]. In general, clusters in a graph represent sets of the graph nodes with more edges inside the cluster than to the rest of the graph. In directed networks, this density-based definition can be extended to a pattern-based definition [40], to highlight the very nature of the links between the cluster nodes. Specifically, in the case of the NBI graph the preliminary cluster analysis identifies the main functions of the system: source of particles, caesium-related aspects, flow of particle current inside the accelerator, heating of surfaces, neutralisation and divergence. Fig. 9 shows that the functional relationship is not limited by the node geography but it involves nodes physically located in different parts of the NBI.

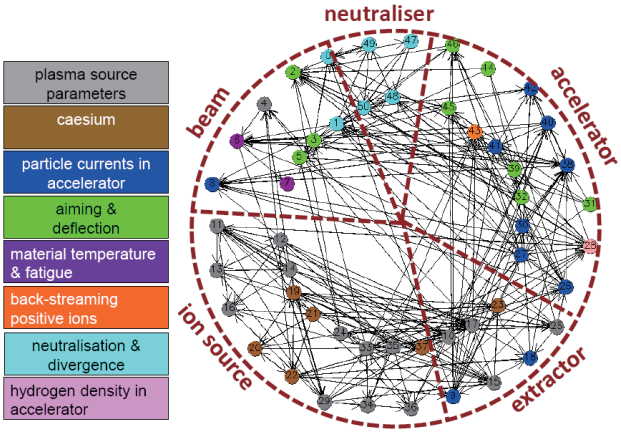

Fig. 9 NBI directed graph clustering based on Markov search.

3.2 NBI controllability and driver nodes

Based on the findings described in the previous section, the graph analysis was extended. One key advantage of representing a system by means of a graph, is that its controllability becomes predictable. Let a system be represented by the linear, time-invariant dynamical relationship $x' = Ax + Bu$, where x is the set of variables specifying the status of the system, x' the time derivative of x, $A = (a_{ij})$ the matrix of the interconnections among the system variables, u the input vector and B the internal nodes controlled by the external inputs; this system is controllable if structurally controllable (namely equivalent to a controllable system, which can be driven from any initial state to any desired final state in finite time) if and only if the matrix $C = (\mathrm{B,AB,A^2B,}\ldots \mathrm{A^NB})$ has rank m [41, 42].

For the NBI the matrix B contains the amount of gas injected in the source and in the neutraliser, the voltages applied by the power supplies to all grids, geometry of the grids and magnetic fields. Direct computation proves that for the NBI the matrix C has maximum rank.

After ascertaining that the system is controllable, the problem arises of finding the minimum set of nodes which

must be directly controlled in order to drive the whole NBI. Recent work in complex networks [43, 44] has shown that the minimum number of driver nodes needed to have full control of the system calls for the identification of the maximum matching of the system, namely the maximum set of links that do not share start or end nodes [45].

3.3 Driver nodes and relevant aspects of the design

Using the method described in [46, 47] the driver nodes for the NBI graph can be identified in parameters of: the particles in the source; caesium and its distribution; deflection of the beam in the accelerator; optics of the accelerator; gas in the accelerator; neutraliser geometry (the driver nodes found in this preliminary analysis are highlighted in Table 1).

The driver nodes essentially represent the most important aspects to be taken care of during the NBI design and also during the NBI operation. Consequently these parameters deserve a special attention in the design and the operation of the diagnostic system, so that the value of the parameters corresponding to the driver nodes are available to the NBI operators.

The present preliminary analysis of the NBI as a complex network has been conducted considering the system at full performances. Of course, dedicated analyses must be applied to the intermediate phases in which only part of the sub-systems will be operating or the whole system will be operated at reduced parameters.

4. Conclusions

The present paper summarises the main features of the design of the high power, high voltage and long pulse NBI for ITER. Specifically the electrostatic and magnetic configurations are described as well as the background gas profile calculations. The NBI system is analysed in terms of the complex network paradigm and its internal features are classified using directed graph theory, which allows the identification of the most relevant phenomena to be controlled during the operation and the required diagnostics.

This work was set up in collaboration and financial support of F4E.

[1] D. Meade, Nucl. Fusion **50**, 014004 (2010).
[2] P. Agostinetti *et al.*, Nucl. Fusion **56**, 016015 (2016).
[3] G. Chitarin *et al.*, Rev. Sci. Instrum. **87**, 02B311 (2016).
[4] G. Serianni *et al.*, Rev. Sci. Instrum. **87**, 02B927 (2016).
[5] E. Sartori and P. Veltri, Vacuum **90**, 80 (2013).
[6] E. Sartori *et al.*, Vacuum **122**, Part B, 275 (2015).
[7] E. Sartori *et al.*, Rev. Sci. Instrum. **85**, 02B308 (2014).
[8] E. Sartori *et al.*, AIP Conf. Proc. **1515**, 121 (2013).
[9] H.P.L. De Esch *et al.*, Nucl. Fusion **55**, 096001 (2015).
[10] E. Sartori *et al.*, Rev. Sci. Instrum. **87**, 02A502 (2016).
[11] M. Dalla Palma *et al.*, Fusion Eng. Des. **96-97**, 557 (2015).
[12] G. Chitarin *et al.*, AIP Conf. Proc. **1655**, 040008 (2015).
[13] P. Franzen *et al.*, Plasma Phys. Control. Fusion **53**, 115006 (2011).
[14] M. Fröschle *et al.*, Fusion Eng. Des. **88**, 1015 (2013).
[15] A. Kojima *et al.*, Nucl. Fusion **51**, 083049 (2011).
[16] M. Kashiwagi *et al.*, AIP Conf. Proc. **1515**, 227 (2013).
[17] E. Sartori and P. Veltri, Vacuum **90**, 80-88, (2013).
[18] G. Chitarin *et al.*, Fusion Eng. Des. **88**, 507 (2013)
[19] V. Antoni *et al.*, Rev. Sci. Instrum. **85**, 02b128 (2014).
[20] W.B. Hermannsfeld, Stanford Linear Accel. Center, Tech. Rep. SLAC-226 (1979).
[21] J. Paméla, Rev. Sci. Instum. **62**, 1163 (1991).
[22] OPERA-3D, Vector Fields Co.Ltd., http://operafea.com/
[23] Y. Takeiri *et al.*, Rev. Sci. Instrum. **66**, 5236 (1995).
[24] P. Agostinetti *et al.*, Nucl. Fusion **51**, 063004 (2011).
[25] P. Veltri *et al.*, IEEE Trans. Plasma Sci. **42**, 4 (2014).
[26] G. Fubiani *et al.*, Phys. Rev. Special Topics Accel. Beams **11**, 014202 (2008).
[27] P. Veltri *et al.*, Rev Sci Instrum. **83**, 02B709 (2012).
[28] E. Sartori *et al.*, Rev. Sci. Instrum. **87**, 02B917 (2016).
[29] E. Sartori *et al.*, IEEE Trans. Plasma Sci. **42**, 3 (2014).
[30] P. Veltri *et al.*, Rev. Sci. Instrum. **87**, 02B313 (2016).
[31] P. Agostinetti *et al.*, Rev. Sci. Instrum. **87**, 02B913 (2016).
[32] P. Veltri *et al.*, Rev. Sci. Instrum. **87**, 02B908 (2016).
[33] P. Agostinetti *et al.*, J. Nucl. Mater. **417**, 924 (2011).
[34] D. Marcuzzi *et al.*, Rev. Sci. Instrum. **87**, 02B309 (2016).
[35] D. Marcuzzi *et al.*, Fusion Eng. Des. **85**, 1792 (2010).
[36] V. Antoni *et al.*, submitted to Plasma Sources Sci. Technol.
[37] J. Bang-Jensen and G.Z. Gutin, *Digraphs* (Springer, London, 2001).
[38] S. Fortunato, Phys. Rep. **486**, 75 (2010).
[39] gephi.github.io: free software for graph analysis.
[40] F.D. Malliaros and M. Vazirgiannis, Phys. Rep. **533**, 95 (2013).
[41] C.-T. Lin, IEEE Trans. Autom. Control **19**, 201 (1974).
[42] R.W. Shields and J.B. Pearson, IEEE Trans. Autom. Control **21**, 203 (1976).
[43] Y.-Y. Liu, Nature **473**, 167 (2011).
[44] Zh. Yuan *et al.*, Nature Comm. **4**, 2447 (2013).
[45] Z. Galil, ACM Comp. Surv. **18**, 23 (1986).
[46] D. Das *et al.*, Network Prot. Alg. **6**, (2014).
[47] A. Chatterjee, ICACCI 2013, 1146.